Astron. Astrophys. 301, 201–212 (1995)

ASTRONOMY AND ASTROPHYSICS

The corona of the young solar analog EK Draconis

M. Güdel[1,2], J. H. M. M. Schmitt[3], A. O. Benz[4], and N. M. Elias II[5]

[1] Paul Scherrer Institut, Würenlingen und Villigen, CH-5232 Villligen PSI, Switzerland
[2] Joint Institute for Laboratory Astrophysics, University of Colorado & NIST, Boulder, CO 80309-0440, USA
[3] Max-Planck-Institut für Extraterrestrische Physik, Giessenbachstrasse, D-85740 Garching, Germany
[4] Institut für Astronomie, ETH-Zentrum, CH-8092 Zürich, Switzerland
[5] United States Naval Observatory, Astrometry Department, Interferometry Divison, 3450 Massachusetts Av. NW, Washington, DC 20392-5420, USA

Received 10 August 1994 / Accepted 24 December 1994

Abstract. First coronal microwave and new soft X-ray observations of the very active, near-Zero-Age Main-Sequence (ZAMS) dG0e star EK Dra = HD 129333 show that this analog of the young Sun is more luminous in both emissions than most single M-dwarf flare stars. Variations in the 8.4 GHz flux include modulation with the optically determined rotation period of 2.7 days. This result points to a non-uniform filling of the corona with energetic electrons due to an incomplete coverage of the surface with active regions and a source volume that is not concentric with the star. The radio luminosity varying between $\log L_R$ = 13.6 and 14.6 (L_R in erg $s^{-1}Hz^{-1}$) shows evidence for unpolarized gyrosynchrotron flares, while strongly polarized flares were absent during the observations. This star is the first young, truly solar-like main sequence G star discovered in microwaves. Having just arrived on the main sequence, it conclusively proves that young, solar-like G stars can maintain very high levels of radio emission *after* their T Tau phase. The X-ray observations were obtained from the ROSAT All-Sky Survey (RASS). The average X-ray luminosity amounts to $\log L_X = 29.9$ (L_X in erg s^{-1}). A Raymond-Smith type plasma model fit yields two plasma components at temperatures of 1.9 and 10 MK, with volume emission measures of 1.2 and $2.5 \cdot 10^{52}$ cm^{-3}, respectively. The X-ray light curve is significantly variable, with the photon count rate from the cooler plasma being strongly modulated by the rotation period; the emission from the hotter plasma is only weakly variable. Modeling of the source distribution in the stellar corona yields electron densities of the order of $4 \cdot 10^{10}$ cm^{-3} or higher for the cool plasma component. It indicates that a considerable portion of EK Dra's high X-ray luminosity is due to high-density plasma rather than large emission volume. Parameters for an X-ray flare indicate an electron density of $1.75 \cdot 10^{11}$ cm^{-3} and a source height of $(1-2) \cdot 10^{10}$ cm, compatible with a few times the scale height of the *cooler* plasma component.

Key words: stars: activity – stars: coronae – radio continuum: stars – X-rays: stars – stars: individual: HD 129333

1. Introduction

The Sun's magnetic activity is thought to originate from an interaction between convection and rotation. Despite its relatively slow rotation and hence modest activity level, the Sun's closeness has allowed us to investigate signatures of magnetic activity in detail and interpret much more active stellar coronae in terms of the solar analog. Outstanding examples of increased coronal activity comprise Me dwarfs (often recognized as "flare stars") or RS CVn binary stars, whose dynamo action is increased by rapid synchronous rotation due to strong tidal interaction. However, a deeper understanding of the evolution of the solar dynamo requires information from *solar proxies* with internal structures, surface gravities, sizes, and masses similar to the Sun's. Observations of such stars have been particularly difficult in the microwave regime. The Sun would appear as a very weak and inactive source even at distances of the nearest stars; its quiescent (thermal) 3.6 cm microwave flux at a distance of 5 pc would be ~ 2 μJy, practically undetectable with present-day radio observatories. The deficiency of microwave-detected G stars suggests that many solar proxies are intrinsically weak radio emitters.

Young G stars in the solar vicinity offer the potential to study the early, more active phases of the solar dynamo. The Pleiades Moving Group (Local Association) is particularly important because the ages of many of its components (around $\sim 50-70$ Myrs) are just slightly larger than the age of solar proxies arriving at the main sequence. In this paper, we present the first coronal microwave observations together with new X-ray data of an outstanding nearby member of this group, EK Dra. The observations were obtained with the aim of i) investigating the coronal activity of the Sun just *after* its arrival on the

Send offprint requests to: M. Güdel

main sequence, ii) deriving the coronal structure of a solar proxy with a strongly enhanced internal dynamo, and iii) comparing the short-term variability of the coronal emissions with that of the present-day Sun and active stars of other spectral types. The star is currently being investigated by extended, pointed ROSAT observations (Dorren et al. 1995).

2. EK Draconis

EK Dra = Gl 559.1 = HD 129333 is a dG0e star that, based on its kinematic properties, belongs to the Pleiades Moving Group (Soderblom & Clements 1987). Its distance is estimated to be 31 pc (Gliese 1969). It has an optical rotation period of approximately 2.7–2.8 days (Guinan & Dorren 1992; Dorren & Guinan 1994 = DG94), suggesting an equatorial rotation velocity of $v \approx 17$ km s^{-1}, in good agreement with the statistical mean of $v\sin i$ for Pleiades-age G stars (Soderblom 1983; we note that $\sin i \gtrsim 0.9$, see DG94). EK Dra's age is of the order of 50–70 Myr (see, e.g., DG94), roughly consistent with the Zero-Age Main-Sequence (ZAMS) age for this spectral type[1]. EK Dra's photospheric spot coverage may amount to some 6%, or about an order of magnitude more than on the Sun during its activity maximum (DG94). Elias & Dorren (1990a,b) report a 14 day (or possibly 28 day) period in the position angle of the optical linear polarization, which they attributed either to circumstellar material or an undetected close stellar companion. DG94 find that the photospheric/chromospheric activity undergoes cyclic variations with an "activity cycle" period of about 12 years. The activity maximum occurred around 1989-1990, while the minimum is expected around 1995. These characteristics make EK Dra an ideal and very active analog of the young Sun at a time when it had just arrived on the ZAMS and was forming its planetary system (DG94).

Observational circumstances are complicated by the probable presence of a distant companion to EK Dra. Long-term CORAVEL radial velocity measurements by Duquennoy & Mayor (1991) indicate a companion with a mass $\geq 0.37\ M_\odot$ in a highly eccentric orbit with an orbit period of approximately 12 years. The mass restriction allows for any spectral type between G and early M. Spectral types earlier than K0 can probably be excluded for spectroscopic reasons. We notice, however, that a late-K to M type companion at the age of EK Dra is likely to be a pre-main-sequence star.

[1] Available (trigonometric) parallaxes locate EK Dra *on* or (inconsistently) even slightly below the ZAMS (cf. DG94; Dorren et al. 1995; SIMBAD entries). EK Dra must thus have arrived on the main sequence recently (DG94); its age is therefore $\gtrsim$30–40 Myrs and is in fact likely to be $\lesssim$100 Myrs (DG94; Barry 1988), also suggested from rotation, lithium abundance, and chromospheric, transition region, and coronal activity (DG94; Soderblom 1985; Soderblom & Clements 1987; Barry 1988; Jeffries & Jewell 1993). This age range is roughly commensurate with the (debated) intrinsic age spread and the age uncertainties of the Pleiades and the α Persei open clusters (members of the Local Association, traditional age values of $\approx$ 70 Myrs and 50 Myrs, with intrinsic age spreads possibly as large as 20-30 Myrs each; see discussion in Soderblom et al. 1993).

EK Dra has further been found to be a strong X-ray source with an X-ray luminosity up to $\log L_X \approx 30$ (L_X in ergs s^{-1} in the ROSAT passband 0.1–2.4 keV; Guinan & Dorren 1992; Güdel et al 1993a, 1994; DG94; Dorren et al. 1995). Dorren et al. (1995) report an apparent decline of the average X-ray luminosity in parallel to the decline of other activity indicators, based on pointed ROSAT observations between 1990 and 1993. EK Dra has also been identified in the ROSAT Wide Field EUV All-Sky Survey (Pounds et al. 1992) as well as in the EUVE All-Sky Survey (Malina et al. 1994). We further notice that L_X and $v\sin i$ approximately fulfil a relation found for many classes of active stars (Pallavicini et al. 1981), and in particular for main-sequence G stars (Dorren et al. 1995).

EK Dra is an obvious candidate to search for solar proxies in microwaves. A VLA[2] detection experiment in January 1993 indeed discovered the star as the first solar-like radio G star just having arrived on the main sequence, with a relatively high 8.5 GHz (3.6 cm) flux level of $S = (0.34 \pm 0.025)$ mJy, corresponding to a luminosity of $L_R \approx 4 \cdot 10^{14}$ erg s^{-1}Hz^{-1} (Güdel et al. 1993a, 1994). Elias & Dorren (1990b) reported upper limits (1σ rms $\approx$ 0.019 mJy), but the older positional catalog information then available was erroneous by $\sim 5''$.

3. Observing programs

3.1. VLA microwave observations

The *microwave* observations presented below are based on four different VLA radio investigations of EK Dra between 1990 and 1993, comprising, to our knowledge, all VLA observations of this star until early 1994. Table 1 contains an observing log of all programs. The observations obtained in 1990 were previously analyzed by Elias & Dorren (1990b). We re-analyzed these data and searched for the star using updated coordinate information (see Sect. 3.3). The detection from January 1993 was previously reported in Güdel et al. (1993a, 1994). The latest observing data set, obtained in September and October, 1993, consists of 36 well separated $\sim$1 hour segments obtained at 3.6 cm (ν = 8.4 GHz) and 6 cm (ν = 5 GHz) wavelengths, including 4 pairs at both wavelengths obtained within $\sim$1 hr. This program was designed to investigate slow variations and rotational modulation.

All observations used standard VLA frequencies with a total bandwidth of 100 MHz. We regularly switched to the NRAO phase calibrator 1435+638 (1358+624 for the 1992 observation). The data were edited, calibrated, and mapped using standard AIPS procedures. Fluxes were determined for map features within $\sim$1/2 FWHM of the true position of EK Dra. We accepted fluxes of such features on a single map as *detections* if they exceeded the 3σ map noise rms, but considered values down to the 2σ level as the *most likely* fluxes for the variability study (the detectability of EK Dra is well established).

[2] The VLA is a facility of the National Radio Astronomy Observatory, which is operated by Associated Universities, Inc., under cooperative agreement with the U. S. National Science Foundation.

Table 1. Observation log for the VLA observations

Date (y/m/d)	UT (hr)	Array Config.	Wavelength (cm)	On-source time (min)	Detected flux (μJy$\pm 1\sigma$)
1990/06/28	4-10	A/B hybrid	2	~60	$< 124 \pm 62$
			3.6	~60	96 ± 18
			6	~60	106 ± 28
			20	~60	$< 144 \pm 72$
1992/01/26	12	B/C hybrid	6	18	150 ± 50
1993/01/29	10-11	A/B hybrid	3.6	45	340 ± 25
1993/09/02-10/15	...	C/D hybrid	3.6 (24 sessions)	~ 40 each	< 40 to 177 ± 31
			6 (12 sessions)	~40 each	< 60 to 200 ± 47

We monitored, as a reference, the flux of a nearby (presumably extragalactic) source and the phase calibrator flux to detect any systematic calibration errors. None were found, with the possible exceptions of four 3.6 cm observations obtained at very low elevations (9–10 degrees, 18 degrees in one case); they show consistently lower phase calibrator and lower reference fluxes, and considerably increased noise rms values. These observations were not considered in our statistical investigation.

3.2. *ROSAT X-ray observations*

The *X-ray* observations presented here were extracted from the ROSAT X-ray All-Sky Survey (RASS); details on the ROSAT satellite as well as the X-ray detector used can be found in Trümper et al. (1991) and Pfeffermann et al. (1986). Specifically, all of the ROSAT All-Sky Survey data were taken with the Position Sensitive Proportional Counter (PSPC) during August 1990 – January 1991 by scanning the whole sky in narrow strips perpendicular to the plane of the ecliptic. Each point in the sky was observed once per satellite orbit (orbit period ~96 minutes) for approximately 30 seconds at maximum.

Due to EK Dra's fortuitous ecliptic latitude of approximately 69 degrees, useful data were obtained during ~5 days. Observing dates were from 1990 November 23, 19 UT, to November 28, 19 UT. The data were analyzed using standard procedures within the MIDAS/EXSAS and XSPEC software packages. An average background obtained 10 arcmins away from the star taken at essentially the same time was subtracted from the data (6–10% of the total count rate). Data points with obvious anomalies (i.e., no exposure and hence no photons) were eliminated from all further considerations.

3.3. *Astrometric considerations*

We encountered considerable uncertainty with regard to accurate coordinates of EK Dra in the available literature. Because of the positional uncertainty and low microwave flux of EK Dra, the observations in 1990 initially yielded a non-detection (Elias & Dorren 1990b). The J2000.0 coordinates for EK Dra in the recently published Hipparcos Input Catalog (HIC; Turon et al. 1992) are R.A.(2000) = $14^h39^m00^s.197, \delta(2000) = 64°17'29''.49$ with proper motions of $\mathrm{pm(R.A.)} \cdot \cos\delta = -0''.138\ \mathrm{yr}^{-1}, \mathrm{pm}(\delta) = -0''.035\ \mathrm{yr}^{-1}$. These coordinates should be accurate within $0''.6$ at the worst (Grenon 1993). With this, the expected position of EK Dra during the January 1993 observation is

$$\mathrm{R.A.}(2000) = 14^h39^m00^s.344, \quad \delta(2000) = 64°17'29''.73 \quad (1)$$

while we found the radio centroid position at

$$\mathrm{R.A.}(2000) = 14^h39^m00^s.351, \quad \delta(2000) = 64°17'29''.89 \quad (2)$$

(see Güdel et al. 1994) implying a deviation of $0''.17$ (mainly in declination); this is negligible and suggests that the HIC coordinates of EK Dra should be adopted.

4. Data analysis and results

4.1. *Components of the microwave emission and variability*

In Fig. 1, the 3.6 cm and 6 cm fluxes for all observations in September-October, 1993, are plotted versus time. We have performed a detailed statistical study of the measured 3.6 cm flux distribution of this sample. We find that the source flux is definitely not constant; rather, we can distinguish between three different modes, signified by "low fluxes" ($\lesssim [50 - 55]$ μJy at the 2σ level), "intermediate fluxes" ($\sim [70 - 100]$ μJy, mean ≈ 80 μJy), and "high fluxes" (≥ 150 μJy). The three states thus indicate intrinsic *variability* of the coronal radio emission. Further, we found that a few of the "high-flux" observations are significantly variable themselves during the observing time of $\sim$ 1 hour beyond statistical fluctuations. They may constitute the peaks of gradual flares with the wings not distinguishable at our signal-to-noise ratio. The strongest fluxes reach up to about (400–500) μJy for a short time, exceeding the quiescent radiation (~ 80 μJy) by a factor of 5–6. No such short timescale variability was identified during any of the lower-flux observations.

No circular polarization was found in any of these events, nor in any of the full observations, with the most stringent 3σ upper limit being 24% for the observation of January 29, 1993. Also, concatenated data sets yielded only upper limits to the degree

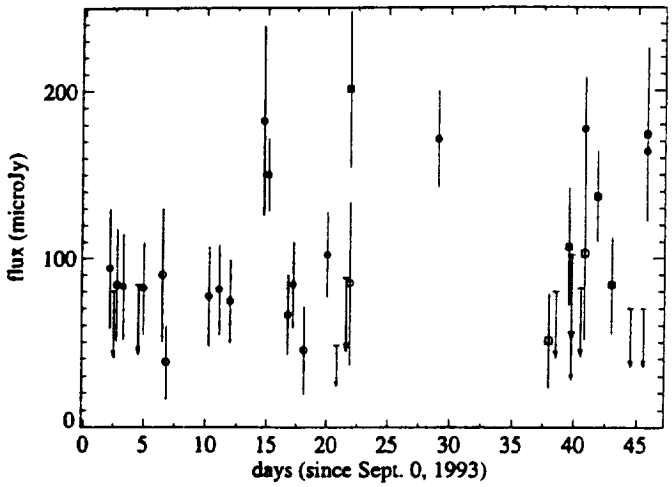

Fig. 1. Microwave flux light curve of EK Dra during the observing campaign in September – October 1993. Circles: 3.6 cm; squares: 6 cm. Filled symbols are $\gtrsim 2.5\sigma$, open circles are $\lesssim 2.5\sigma$ estimates. Upper limits (arrows) refer to 3.6 cm before day 25, and to 6 cm thereafter; additionally, the more stringent upper limit on day 39 (October 9) is for the 3.6 cm observation. Error bars are 1σ rms read from the map background

of circular polarization, with a polarization degree of $< 13\%$ for the summed "high-flux" 3.6 cm data in September-October 1993.

Most of the 6 cm observations in the 1993 data set were obtained during a time when the 3.6 cm flux was predominantly high (October); the increased noise rms at 6 cm does not allow us to separate the 6 cm fluxes into activity modes. Three of our four 6 cm–3.6 cm pairs contain detections. Estimates for the spectral index α in $S \propto \nu^{\alpha}$ range between −1 and values compatible with 0 (also for the 1990 observation, see Table 1). We caution, however, that the signal-to-noise ratio in each observation is small, and that the observations were obtained only consecutively within $\sim$ 1 hour.

4.2. *Period analysis of the "quiescent" microwave emission*

Except for the flare-like events on September 14/15, all 3.6 cm fluxes during September 1993 are either intermediate or low (Fig. 1). Accepting the variable and apparently flaring characteristics of the high-flux category, we will not use fluxes exceeding $\sim$130 μJy in the following analysis. To search for periodic modulation in the radio data, two statistical methods were applied after folding the light curve with an arbitrary period; for both methods, minima of the statistics indicate possible periods (for details, see Appendix). The results are plotted in Fig. 2a,b as a function of assumed period.

We find overall agreement between the two methods. The statistically most significant ($> 99.5\%$ confidence limit in method 'A') and broadest signal in *both* plots occurs at a period of $P = 2.73$ days; it has the "low-flux" points sharing the same *phase* interval of about 20%–40% length, completely separated from the "intermediate-flux" points, which share the

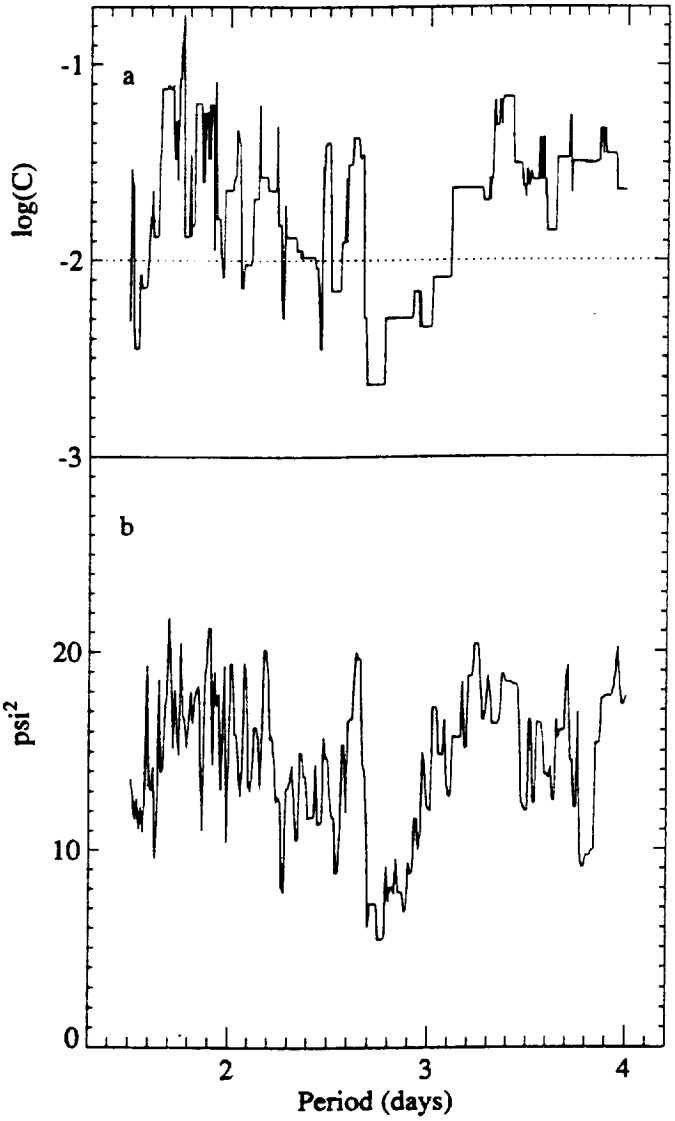

Fig. 2a and b. Period analysis for the low- and intermediate-flux 3.6 cm data from September – October 1993. **a** Confidence values $C(P)$ for the zero hypothesis of one parent population for two phase range partitions; minimum C for any partition using rotation period P is given. $1 - C$ gives the confidence level for significantly different samples. For illustration, $\log C$ is shown (method A; see Appendix). **b** $\psi^2(P)$ for point-to-point variability (method B; see Appendix, Eq. A3). – The sampling theorem restricts reliable identifications to $\gtrsim 1.5$ days. For both statistics, the minima suggest possible rotation periods. In (**a**), the dashed horizontal line indicates the critical confidence level adopted for consideration of periods as possibly significant

remaining 60%–80%. No similar statement can be made for the other candidate periods.

Thus, if the data are governed by any periodicity, $P_{\rm rot} = (2.73 \pm 0.04)$ days is the most likely period (the error gives the total allowed range in which the two categories of flux points are separated in phase), and its value corresponds exactly to the optically determined rotation period of the G star, i.e. (2.75±0.05) days (DG94). We explicitly checked whether the assumption of microwave modulation with the *optical* rota-

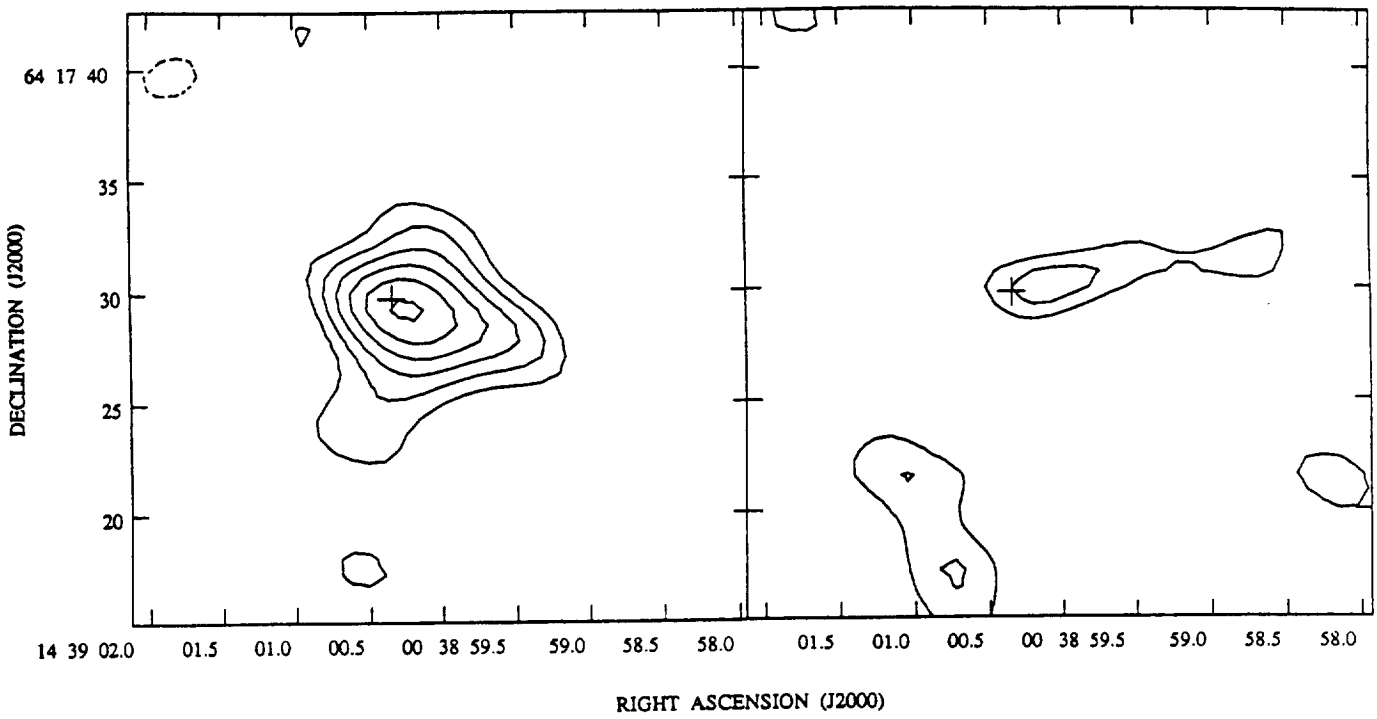

Fig. 3. VLA 3.6 cm maps obtained by concatenating data in the intermediate-flux phase interval (left) and data pertaining to the low-flux phase interval (right). Contours are separated by 10 μJy $\approx 1\sigma$ on *both* maps. The lowest contour is at 2σ, the dashed contour defines -2σ. The non-elliptical shapes of the stellar images are due due to underlying noise features at the $\sim 3\sigma$ level. Crosses give the optical position (see Sect. 3.3)

Table 2. Results from X-ray spectral fit (90% confidence limits)

Parameter	Value
Hydrogen column density n_H	$(1.21^{+3.03}_{-1.21}) \cdot 10^{19}$ cm^{-2}
Component 1: Temperature T_1	$(1.90^{+.86}_{-.52}) \cdot 10^{6}$ K
Component 1: Emission measure EM_1	$(1.17^{+.41}_{-.37}) \cdot 10^{52}$ cm^{-3}
Component 2: Temperature T_2	$(1.03^{+.17}_{-.18}) \cdot 10^{7}$ K
Component 2: Emission measure EM_2	$(2.48^{+.75}_{-.67}) \cdot 10^{52}$ cm^{-3}
fit χ^2/degrees of freedom	15.8/19

tion period of the G star finds *direct* and unbiased support from the data. We concatenated observations belonging to each of the two phase intervals mentioned above, assuming a rotation period of 2.73 d. The star was thus detected at a barely significant level of (34±11) μJy in the lower-flux phase interval, while the complementary interval yields a prominent detection at (77±9) μJy (Fig. 3). We conclude that EK Dra's radio emission is likely to be subject to hemispheric variations compatible with the rotation of the G star.

4.3. Spectral results from the X-ray observations

In Fig. 4 we show the RASS X-ray light curve obtained for EK Dra. Specifically we show in Fig. 4a the overall PSPC light curve, which is split up into a hard (PSPC channels 42–201, energy 0.4–2 keV) and a soft (channels 11–41, energy 0.1–0.4 keV) light curve in Fig. 4b and 4c, respectively. The X-ray light curves show two main features: i) A slow modulation predominantly in the soft channels, and ii) a few rapid excursions (e.g., events labeled 'A', 'B', 'D') that may be individual flare events.

The complete X-ray survey data set contained enough ($\sim$ 1000) photons to construct a pulse-height spectrum and perform a spectral analysis. We used optically thin Raymond-Smith type plasma models folded with the ROSAT PSPC response. Applying a one-temperature model yielded unacceptable results ($\chi^2 \gtrsim 87$ for 25 energy bins). Acceptable fit results were obtained by fitting two temperatures, two corresponding emission measures, and the hydrogen column density. The results are reported in Table 2 and Fig. 5. We notice that very similar results were reported for *pointed* ROSAT PSPC observations (Dorren et al. 1995). The parameters are also reminiscent of coronal parameters of other active late-type stars in that the higher-temperature component (around 10^7 K) is the dominant source of emission measure (see Schmitt et al. 1990). The derived hydrogen column density is not statistically significant. The integrated flux in the ROSAT energy range, 0.1–2.4 keV, yields a total, average X-ray luminosity of $\log L_X = 29.92$, which exceeds typical X-ray luminosities of late-type dwarf stars and in particular that of the Sun ($\log L_X \approx 27.3$); it also exceeds the *average* X-ray luminosities of G stars in the Pleiades cluster ($\log L_{X,mean} \approx 29.5$;

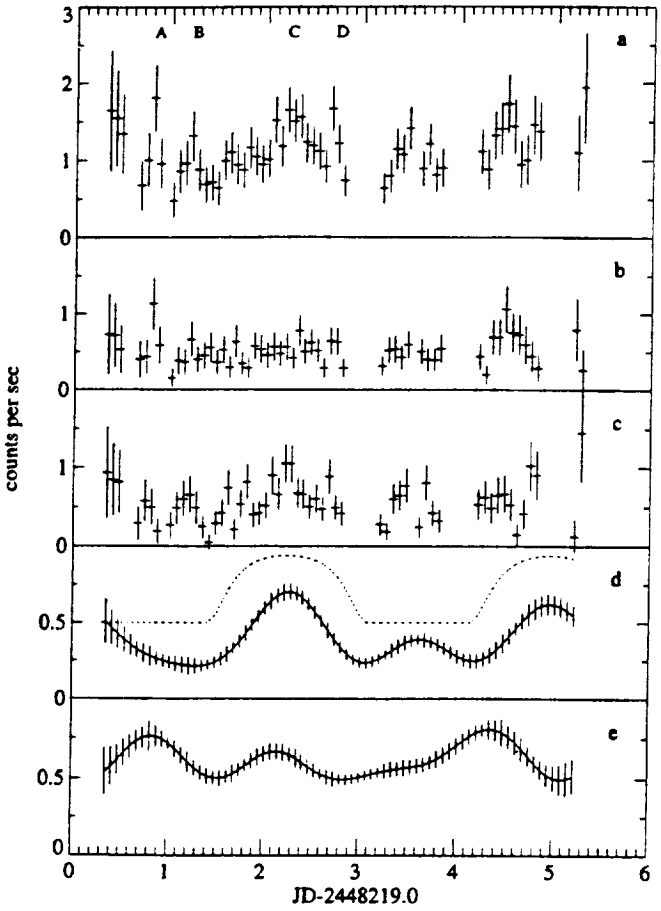

Fig. 4a–e. ROSAT All-Sky Survey X-ray light curve of EK Dra; bin separation is approximately 96 minutes. **a** All photons; **b** hard channel (0.4–2.4 keV); **c** soft channel (0.1–0.4 keV); **d** low-pass filtered light curve from cool (2 MK) plasma; the dashed line represents a model simulation (see Sect. 5.3), shifted by +0.5 cts s^{-1} for illustration; **e** low-pass filtered light curve from hot (~10 MK) plasma. Notice that slow variations are predominantly due to soft photons originating from the cool plasma, while the flare-like event 'A' appears to be hard

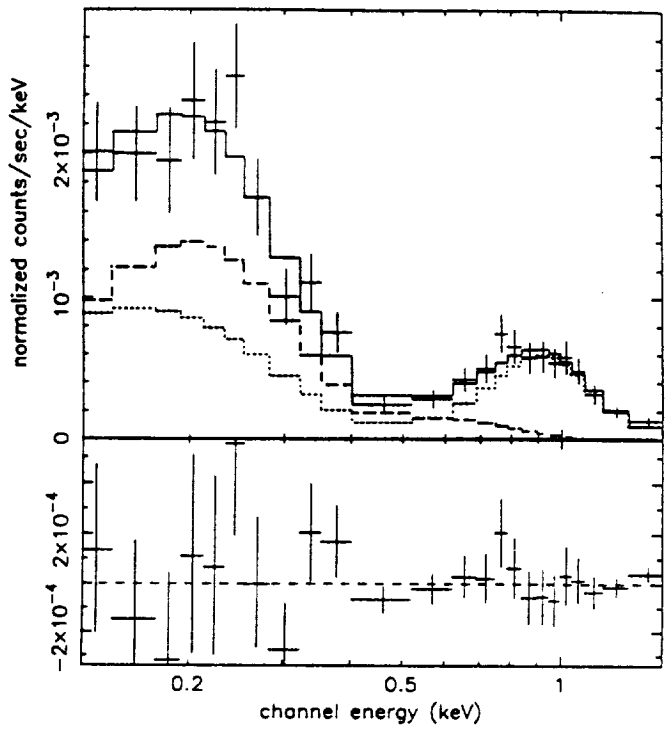

Fig. 5. Pulse-height spectrum (crosses) and two-component fit (histogram) of full ROSAT X-ray data set. For fit parameters, see Table 2. Dashed/dotted spectra models are based on the radiation from the cool/hot plasma, respectively. The lower panel shows residuals (observation minus fit)

Micela et al. 1990; Schmitt et al. 1993; Stauffer et al. 1994). At the modulation peaks, EK Dra yields $\log L_X = 30.1$.

We modeled the relative contributions of each plasma component to the hard and soft channels for fixed temperatures $T_{1,2}$. By inversion of the equation system, we can derive two photon light curves C_{hot} and C_{cool} corresponding to the emission from the hot and the cool plasma ($C_{cool} = 1.39 \cdot C_{soft} - 0.69 \cdot C_{hard}$ and $C_{hot} = 1.69 \cdot C_{hard} - 0.39 \cdot C_{soft}$). We find, as shown in Fig. 4d-e, that the emission from the hot plasma remains effectively constant, while, surprisingly, *the cool plasma is responsible for the modulation*. The flare-like event 'A', on the other hand, shows up as a significant event in the (unfiltered) C_{hot} only.

4.4. Periodicity in the X-ray light curve

The low-pass filtered light curve of Fig. 4a (similar to Fig. 4d) shows two maxima separated by $P = 2.6$ to 2.7 days; an autocorrelation analysis shows a broad secondary maximum around $P = 2.53$ days, including the optical rotation period of 2.7 days. Similarly, the interval between the two maxima in the C_{cool} light curve (Fig. 4d) is close to 2.7 days.

Support for these results comes from a folding analysis of the X-ray photons. By varying the folding period, the phase bin arrangement that is least compatible with the assumption of constant flux was determined (in the sense of χ^2 statistics). The phase plot is shown in Fig. 6 and clearly indicates a smooth and periodic variation. The optimum period in this case (20 phase bins) is 2.6 days. By varying the number of phase bins, we found a scatter of the optimum period of about ±0.4 days. This is plausible because we estimate that there is a phase uncertainty of $\pi/2$ between the beginning and the end of the light curve (see Fig. 4). With $f = P^{-1} = 0.385$ (for $P = 2.60$ days), $df = (4T)^{-1} = 0.05$, the confidence period range becomes (2.3 – 3.0) days.

5. Discussion

5.1. Microwave emission mechanism

The brightness temperature T_B of the microwave emission can be estimated by assuming that the star is covered with active regions. A ZAMS solar analog is somewhat smaller than the present Sun, but the height of the corona is expected to be of the order of 0.1 stellar radii at the minimum (see also Sect. 5.3

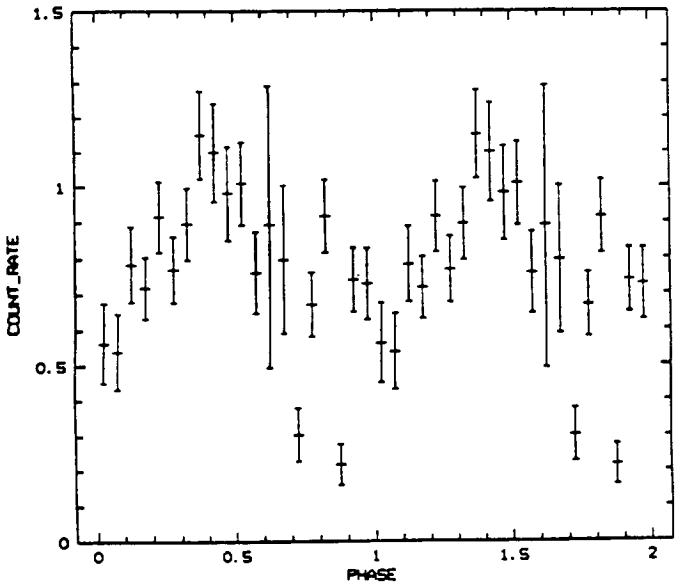

Fig. 6. Phased X-ray light curve using folding of all photon arrival times with a selectable period and subsequent binning in phase space. The optimum period determined with a maximizing χ^2 procedure (period least compatible with constancy) for this representation is 2.6 days

below); we therefore assume a source radius r equal to one *solar* radius ($=7 \cdot 10^{10}$ cm). The brightness temperature T_B is

$$T_B = \frac{Sc^2}{2k\nu^2\Omega}, \quad (3)$$

where S is the measured flux density, (1 μJy = 10^{-29} erg cm^{-2}s^{-1}Hz^{-1}), c is the speed of light, k is Boltzmann's constant, and $\Omega = \pi r^2/d^2$ is the solid angle of the source as seen from Earth. With $d = 31$ pc $= 9.58 \cdot 10^{19}$ cm and $\nu = 8.5 \cdot 10^9$ Hz (wavelength of 3.6 cm), $T_B \approx 2.69 \cdot 10^5 S_{\mu Jy}$. During the brightest emission in January 1993, $T_B \approx 9.4 \cdot 10^7$ K, while the quiet level in September 1993 corresponds to $T_B \approx 2.2 \cdot 10^7$ K. Similarly, for 6 cm $T_B \approx 7.93 \cdot 10^5 S_{\mu Jy} \approx 1.2 \cdot 10^8$ K for a typical 6 cm flux of 150 μJy. The brightness temperature provides a lower limit to the effective temperature T_{eff} of the emitting electrons if the plasma is optically thin to the radiation and the emission process is incoherent. In the case of optically thick emission, $T_B = T_{eff}$. Since our radio brightness estimates are much higher than the electron temperatures derived from the ROSAT observations and much larger microwave source radii are required to obtain equality, we conclude that the emission cannot be due to thermal emission from the X-ray emitting plasma. It is also likely that the emitting regions are at least somewhat localized on the stellar surface, as suggested from the rotational modulation; this supports an even higher T_{eff}, since the emission volume would be smaller than assumed above.

The radio-emitting electrons must therefore belong to a very hot, tenuous (not X-ray detected) plasma component, or to a nonthermal population of accelerated electrons. Observations of many active stars (late-type main-sequence, RS CVn binary systems, etc.) clearly support the nonthermal model, invoking gyrosynchrotron emission by mildly relativistic electrons as the likely emission process (cf. review by Güdel 1994). Stellar quiescent radiation at 3.6 cm seems to be predominantly optically thin as judged from spectral observations (cf. Güdel 1994), thus further increasing T_{eff} above T_B. Since the emission is broadband, not strongly polarized, and with a rather flat or slightly decreasing spectrum, the most likely emission mechanism is nonthermal gyrosynchrotron radiation.

5.2. *Microwave and X-ray flares*

EK Dra has not shown any evidence for short timescale, highly polarized, narrow-band radio bursts with large T_B. That kind of flaring microwave emission is frequently observed on active dMe stars ("flare stars"). In fact, hardly any unpolarized, slowly varying flares have been reported from these stars (e.g., Güdel et al. 1995). Polarized, high T_B flares require a coherent emission mechanism, e.g. the electron cyclotron maser instability at the fundamental or the second harmonic of the gyrofrequency $\Omega_c = eB/mc \approx 2.8 \cdot 10^6 B$. For EK Dra's highest flare-like fluxes of ~ 500 μJy at 3.6 cm wavelength, the brightness temperature becomes (under the assumptions in Sect. 5.1) $T_B \approx 1.3 \cdot 10^8$ K, which is, together with the lack of detected circular polarization, compatible with gyrosynchrotron radiation emitted by mildly relativistic electrons.

Our target's low-level and flaring emission is thus more consistent with quiescent emission and flares from RS CVn binaries and solar microwave flares. These flare types involve predominantly incoherent, nonthermal gyrosynchrotron emission from electrons trapped in magnetic fields of a few 10–100 G. The deficiency of polarized flaring 4.9–8.5 GHz emission may thus indicate weaker coronal magnetic fields in the emitting source, placing the second harmonic of the gyrofrequency at lower frequencies (see review by Bastian 1990). Notice that RS CVn binaries also typically belong to spectral classes G and K. Strongly polarized flares thus appear to be more common on the cooler M dwarfs.

In the X-ray light curve, only a few short-timescale events are recognized to be significant, like events A, B, and possibly D in Fig. 4a. We briefly discuss the most outstanding event A. Although its formal significance is marginal in Fig. 4a, i) its development is consistent with flare behavior, ii) it is recognized as a "hard" event (Fig. 4b), and iii) it is recovered as a significant event in the "hot photon light curve". These properties suggest heating by a flaring event to temperatures at or in excess of 10 MK. From the "hard" and "hot" light curves, the e-folding decay time τ is found to be between 60 and 90 minutes. The peak amplitude of ~ 1 ct s^{-1} corresponds to $1 \cdot 10^{30}$ erg s^{-1} if $T = 25$ MK. Consequently, the total released soft X-ray energy is estimated to be between 3.6 and $5.4 \cdot 10^{33}$ erg, one to two orders of magnitude more than in very strong solar X-ray flares.

Assuming radiative cooling, we can derive the flare plasma electron density n_e through $\tau = 3kT/(n_e \Lambda(T))$ with the cooling function $\Lambda(T) = 10^{-24.73} T^{1/4}$ erg cm^{3}s^{-1} for $T \geq 20$ MK (van den Oord & Mewe 1989). The peak flare temperature is unknown; we assume, as a probable lower limit, 25 MK. With

τ = 4500 s, this yields $n_e \approx 1.75 \cdot 10^{11}$ cm^{-3}. The total flare emission measure is observed to be $8.8 \cdot 10^{52}$ cm^{-3}, and thus the flare volume $V \approx 2.9 \cdot 10^{30}$ cm^3. Approximating the flare source with a half-sphere homogeneously filled with plasma and the sphere center on the photosphere, we obtain a likely lower limit for the source height, $h \approx 1.1 \cdot 10^{10}$ cm. A more probable arrangement is a half-circular flaring magnetic loop, for which we assume constant n_e and a constant (circular) cross section with a diameter of 0.1 times the loop length. With this, the (single) loop height becomes $\sim 2.3 \cdot 10^{10}$ cm. For a loop arcade, loop heights between these two extremes are expected. Notice that the pressure scale heights of the quiescent 2 MK and 10 MK plasma components are $H_p = 7.8 \cdot 10^9$ cm and $H_p = 3.8 \cdot 10^{10}$ cm, respectively. For a hydrodynamically stable pre-flare loop, $h \lesssim (2-3)H_p$ (Serio et al. 1981). The flare loops thus have sizes of the order of preflare loops of the *cool* plasma component.

5.3. *Rotational modulation and a model of the cool X-ray component*

Some limited information on the X-ray source distribution can be extracted from the variability in the ROSAT X-ray light curve. Specifically we are interested in constraints on the X-ray emitting coronal volume V *occulted* by the star, since this can be used, in combination with the determined emission measure, to infer plasma densities. We pursued two approaches to accomplish this goal: We first derived model-independent upper limits of the source volume responsible for the *variable* portion of the light curve, and then, in a second step, we confined the source extent ever further in a more realistic albeit still quite simplistic model for the spatial distribution of the X-ray emitting gas. The inclination i of the stellar rotation axis with respect to the line of sight is an important input parameter; we formally adopt i = 60 degrees, but will extend our calculations to other values of i as well.

First, we derived an analytical expression for the total coronal volume V that remains *invisible* for at least a given fraction of P_{rot} (without any constraints for the source height; see Güdel & Schmitt 1995). We did not consider the volume that remains invisible at all phases, since it is intrinsically unobservable and does not contribute to the observed emission. If we interpret the (spectrally soft and not flare-like) bump between day 1.5 and day 3 in Fig. 4 as being due to rotational modulation, the source of this X-ray modulation is visible during t_v = 60% of the rotation period at most, and invisible during the remaining 40%. The total volume V occulted during 40% of the rotation is thus an upper limit to the true volume responsible for the observed modulation. If the modulation is ascribed to the cool plasma component (increase of $\sim$0.6 cts s^{-1}), then a lower limit of the electron density n_e can be obtained from V and the emission measure in Table 2; for i = 60 degrees, we obtain $n_e > 2.5 \cdot 10^{10}$ cm^{-3}; for larger inclination angles i, n_e is larger, reaching $6 \cdot 10^{10}$ cm^{-3} for i = 90 degrees. In this calculation constant density throughout the source region has been assumed. The main result of this model-independent calculation is that for any realistic values of i, the *modulated* part of the light curve comes from a *high-density* region, with densities up to an order of magnitude higher than solar active region densities.

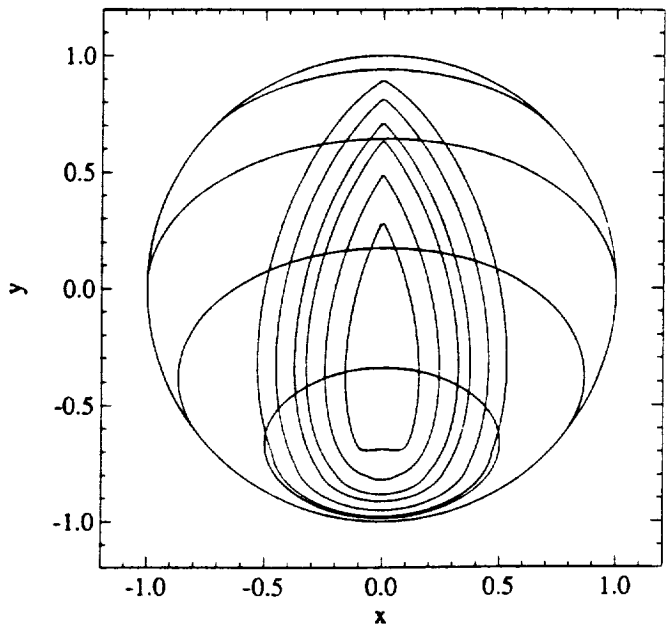

Fig. 7. Maximum extent in longitude and latitude of an X-ray source (symmetric to a fixed meridian) that is visible during 60% of the rotation. The distribution of individual sources within the outlined areas is left unspecified. Stellar inclination is assumed to be 60 degrees. The source heights are, for decreasing source area, h = 0.001, 0.01, 0.03, 0.05, 0.1, and 0.2 stellar photospheric radii. Within a horizontal distance of h to the area borders, the height drops from h to zero (quarter-circular cross section). No solutions exist at latitudes above $\sim$ 25 degrees. In this sketch, the star is viewed from a latitude of –40 degrees, and latitude parallels shown are at –60, –30, 0, and +30 degrees. Sources in the $\sim$ half-circles centered on the south pole remain invisible during the star's rotation

The invisible volume computed above is not restricted in height; in fact, for small phase angles ϕ and/or small inclinations i it becomes infinitely large. In order to obtain a physically more realistic model, we modeled the maximum extent of a single, *connected* source layer of given height h such that the source is *visible* for a specified fraction of P_{rot} ($t_v = 0.6P_{rot}$ in our case; Güdel & Schmitt 1995).

Figure 7 shows the maximum extent of the connected source area. Sources contributing to the bump in the X-ray light curve should be located within the area outlined by the solid lines. The half-circle areas around the south pole are regions where sources are invisible during the whole rotation, and these intrinsically unobservable volumes are again excluded from consideration. Assumed heights are 0.2, 0.1, 0.05, 0.03, 0.01, and $0.001 \cdot R_*$ (for contours with increasing source area). The modeled and re-normalized light curve is plotted dashed in Fig. 4d; while the observations are qualitatively represented, the variation of h mainly results in a different flux re-normalization, so that information on h cannot be gained from such fits. Also, the

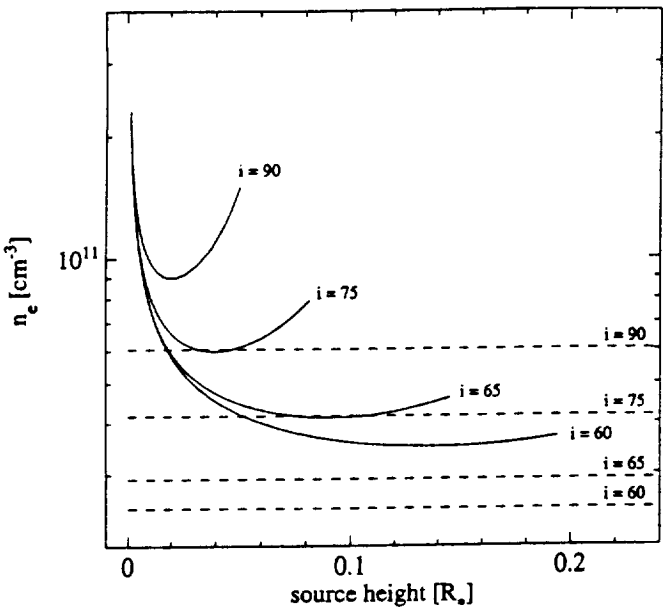

Fig. 8. Electron density n_e of the cooler X-ray plasma component as a function of the geometric height h of the emitting layer (as far as solutions exist; h in units of 1 stellar radius = $6.44 \cdot 10^{10}$ cm), assuming a visibility duration of 60%. The density has been derived from the geometric modeling (Fig. 7), the average emission measure of the cool plasma component (Table 2), and the maximum variation of the count rate in the bump between days 1.5 and 3 in Fig. 4. Assumed inclinations are i = 60, 65, 75, and 90 degrees. Both for very small and large h, the emitting volume decreases (small height and small surface area, respectively), and hence the density increases. The dashed lines indicate the lower limits to the densities based on the model-independent maximum co-rotating atmospheric volume of invisibility during a phase rotation of 0.4 (see text). Tick marks on the density axis are in steps of 10^{10} below 10^{11}

fit light curve is shallower, indicating an even more compact source in the observations. A source height of $0.2R_*$ requires a slightly broadened half-sphere source near –60 degrees latitude (Fig. 7), greater source heights produce less modulation than observed. More likely, the dominant portion of the modulated cool plasma radiation stems from heights $h \lesssim 0.1R_*$; these sources may thus be similar to magnetically confined plasma in active but non-flaring regions on the Sun.

From this model the *instantly* visible volume V_{max} at *maximum* was determined. For i = 60 degrees, V_{max} is obtained for a source layer height of $0.14R_*$ (which incidentially corresponds to the pressure scale height of a 2 MK plasma). The corresponding (minimum) electron density becomes $n_e \approx 3.5 \cdot 10^{10}$ cm^{-3}. Here, we have assumed constant density throughout the source as before. The functional dependence $n_e(h)$ is illustrated in Fig. 8 together with the model-independent lower limits derived above. Increasing i towards 90 degrees increases the minimum electron density to 10^{11} cm^{-3} for the cool plasma alone, and decreases acceptable source heights to values around $0.02R_*$ (see Fig. 8 for i = 65, 75, and 90 degrees; notice that i = 60 degrees is the very lowest limit compatible with observations; DG94). Further, if the variability were due to *all* plasma, then 1.45 times larger densities would be obtained. We conclude, in agreement with the model-independent estimates, that source electron densities are likely to exceed values around $4 \cdot 10^{10}$ cm^{-3}, i.e., to exceed solar active region densities by up to one order of magnitude, while source sizes in this regime are solar-like, i.e., of the order of $0.1R_*$, and comparable with the pressure scale height of the $\sim$ 2 MK plasma. This result indicates that a considerable portion of EK Dra's high X-ray luminosity from the *cooler* component is due to high-density plasma rather than very large volume. In order to balance the thermal pressure, the magnetic pressure, $p_m = B^2/(8\pi)$, in the coronal loops must be larger by typically a factor of 100. With this, we obtain rough estimates for the lower limit of average magnetic fields in the cooler plasma component, $B \gtrsim 240$ G.

The weak or absent modulation in the hotter component allows for different possibilities: i) Much of the hotter material may coincidentally be located at stellar latitudes above $\sim$ 60 degrees and may thus not be subject to occultations; such arrangements would not exclude hot, compact regions. ii) The hotter material may be distributed more homogeneously around the star at any latitude; iii) the hot material is at greater heights, e.g. filling the extended apex volumes of high loops. It may indicate that the luminosity of the high temperature plasma is controlled by large volumes rather than high densities.

5.4. The G star and its companion

Although the unidentified companion undoubtedly contributes some X-ray and radio emission, we argue against that probably cooler star as the *dominant* source of the observed coronal emission and favor the G star for the following reasons:

i) We have identified modulation both in X-rays and in the microwave light curves with a period that matches the optically determined rotation period of the G star ([2.73±0.04] d for the radio data, $2.6^{+0.4}_{-0.3}$ d for the X-ray data, while optically, P_{rot} = [2.75 ± 0.05] d; see DG94). We find it rather unlikely that a distant later-type companion that is not tidally locked to the G star has the *same rotation* period, since the G star must have passed through an episode of strong magnetic breaking and thus spin-down after it arrived on the main-sequence. This evolution history will be completely different and considerably delayed for a later-type star.

ii) EK Dra's X-ray luminosity of $\sim 10^{30}$ erg s^{-1} exceeds the X-ray luminosity of M dwarfs in the Pleiades (or in other open clusters of young age). Almost all detected M dwarfs in the Pleiades have $\log L_X \lesssim 29.5$; a few early K stars exceptionally reach $\log L_X \approx 30$, while the majority has $\log L_X < 29.5$ (e.g., Stauffer et al. 1994). It is in fact the group of G stars that yields the highest X-ray luminosities, with many stars in the range $29.5 \lesssim \log L_X \lesssim 30.5$ (Micela et al. 1990; Schmitt et al. 1993; Stauffer et al. 1994; the average of L_X for the Pleiades G dwarfs is lower, $< \log L_X > \approx 29.5$).

iii) Güdel et al. (1993b) report a linear relation between radio (4.9–8.5 GHz) and X-ray (0.1–2.4 keV) luminosities of active M dwarfs in the range $12 \lesssim \log L_R \lesssim 14.5$, $\log L_R \approx \log L_X - 15.5$. This relation applies to K stars (Güdel 1992) and

extends to other classes of active stars (Drake et al. 1989; Güdel & Benz 1993). It even applies to solar flares, which are sources of coronal heating and microwave gyrosynchrotron emission (Benz & Güdel 1994). On EK Dra, our count rates translate to $\log L_X = 29.65$–30.1. We would thus predict microwave luminosities between $\log L_R = 14.15$ and 14.6 at frequencies between between 4.9 and 8.5 GHz. The observed radio luminosities are at $\log L_R = 13.6$ (minimum phase at 3.6 cm), 14.0 (average quiet level at 3.6 cm), 14.3 (high-flux 3.6 cm/6 cm emission in September and October 1993), and 14.6 (3.6 cm observation in January 1993). We notice that the X-ray and radio luminosities were not measured contemporaneously, and that effects due to the possible activity cycle in the corona (the X-ray observations were obtained during the activity maximum) and shorter-term variability like flares are crucial for a precise comparison. Further, the relation corresponding to the M dwarfs allows for deviations within typically a factor of two or three. Considering these uncertainties, the agreement between observation and prediction is in fact excellent, suggesting that X-rays and microwaves originate from the same star.

We therefore conclude that the X-ray and radio emission in fact come from the G star. Yet, an understanding of the nature of the cooler companion star is crucial for a proper understanding of this stellar system.

6. Summary and conclusions

The active G star EK Dra can be considered to be a solar proxy shortly *after* its arrival on the main sequence. Its properties should be close to those of the young Sun at the time of formation of the planetary system (DG94). High-energy processes on the young Sun are particularly important for an understanding of early processes in the planetary atmospheres (DG94). Our radio observations have been obtained over a portion of the magnetic activity cycle, and the X-ray data stem from the activity cycle maximum (DG94). Results may be summarized as follows:

(1) EK Dra is a steady coronal emitter in the microwaves and soft X-rays. Radio and X-ray luminosity levels are $10^{13.6-14.6}$ erg s^{-1} Hz^{-1} and $10^{29.65-30.1}$ erg s^{-1}, respectively. These values are approximately 2500 and 400 times higher than corresponding values of the quiet Sun. Both also exceed the luminosities typically reported for very active M dwarf flare stars. This parallels extreme chromospheric and transition region activity as reported by DG94.

(2) EK Dra is the first truly solar-like G star at an age just slightly larger than age(ZAMS) that has been discovered as a radio source (Güdel et al. 1993a, 1994). The repeated detections reported in this paper and the near-ZAMS age of EK Dra conclusively prove, for the first time, that solar-like G stars can maintain very high levels ($> 10^3$ times solar values) of both quiescent and probably flaring radio emission for some time *after* arrival at the ZAMS.

(3) Both coronal emissions are significantly variable, with the most prominent variability timescale due to the star's rotation ($P_{rot} = 2.7$ days). Rotational modulation leads to radio and X-ray flux variations within a factor of two approximately. It implies that the emission sources are non-uniformly distributed above the stellar surface.

(4) In our observation, the soft X-ray rotational modulation stems predominantly from the cooler plasma at a temperature of ~ 2 MK. The emission from the hotter material (~ 10 MK) was approximately constant during the rotation. We interpret the cooler material in terms of nonflaring active regions similar to those on the Sun. The interpretation of the observed variations as rotational modulation leads to electron densities of the modulated emission component of at least $\sim 4 \cdot 10^{10}$ cm^{-3}, while our estimates of source visibilities for the cooler component require X-ray source heights of $\sim 0.1 - 0.2$ stellar radii or less. This agrees well with the pressure scale height of the cooler plasma and with solar active region source heights. These results suggest that a considerable portion of EK Dra's *high X-ray luminosity from the cooler plasma portion is due to high-density plasma rather than large emission volumes, while the luminosity of the hot component may be governed by large volumes.* This implies average magnetic fields in the cooler plasma of 240 G or more.

(5) Other variability timescales include flares. In contrast to active, flaring dMe stars, no highly polarized, rapid radio bursts were found during the total of ~ 30 hours of observing time, suggesting weaker source magnetic fields than in dMe stars. Slow flux increases by factors of $\sim 2 - 5$ over the quiescent level were interpreted as gyrosynchrotron flares with brightness temperatures of $T_B \lesssim 1.3 \cdot 10^8$ K. One X-ray event revealed a timescale of $\sim$1 hour, and a peak luminosity of $\sim 1 \cdot 10^{30}$ erg s^{-1}. It is dominated by hard photons and consequently, hot plasma. The total released soft X-ray energy is estimated at $(3.6 - 5.4) \cdot 10^{33}$ erg. The inferred electron density in the flare region is, assuming radiative cooling, $n_e \approx 1.75 \cdot 10^{11}$ cm^{-3}, and the flare source height is of the order of $(1-2) \cdot 10^{10}$ cm^3, compatible with the height derived for the cool plasma component and in rough agreement with the pressure scale height of the cooler, quiescent plasma component. This suggests that the pre-flare loops were located in an area of increased density of cool, non-flaring, active regions.

(6) We argue that the bulk of the coronal emission originates from the G star and not a poorly known distant companion recently identified in radial velocity measurements.

Acknowledgements. The ROSAT project has been supported by the Bundesministerium für Forschung und Technologie (BMFT) and the Max-Planck-Gesellschaft (MPG). We acknowledge the support of our colleagues from the MPE ROSAT group. Ed Guinan stimulated this investigation through many discussions on EK Dra's properties. We thank Michel Grenon for providing us with data from the Hipparcos Input Catalog, and the referee of our paper, Roberto Pallavicini, for many helpful suggestions. We are grateful to the VLA staff for continuous support of and help on this project, and thank Barry Clark for his efforts to establish a valuable observing schedule for the monitoring observations. We further acknowledge support from MPE and ESO in the use of the MIDAS/EXSAS data analysis package for the ROSAT data. MG acknowledges the hospitality of the Institute of Astronomy

of ETH Zürich, where part of this work was carried out. We made use of the SIMBAD data base, operated by CDS, Strasbourg, France. This work has been supported by the Swiss National Science Foundation (grants 8220-033360 and 20-040336.94) and by NASA grant NAG5-2075 to the University of Colorado.

Appendix: statistical variability tests

We searched for periodic variability in the 3.6 cm radio data using the following two methods:

Method A) Complementary phase ranges. We subdivided the phase range [0,1], defined by a trial period of rotation, into two contiguous, complementary phase partitions and computed the weighted average of all stellar fluxes within each partition. A two-tailed Student T-test for samples with unequal variances (see below) will show whether the two averages belong to the same parent population. For two of the low fluxes, we conservatively used their 2σ upper limits as flux estimates. Folding periods were selected in steps of 0.005 days, from 1.5 to 4 days. The smaller phase partition was specified with a selectable width of 0.20, 0.22, 0.24,...,0.50, the larger was defined as its complement. The partitions were shifted through the phase range in steps of 0.02. We take a T-test confidence level of $C \leq 0.01$ as an indication for the two samples to belong to different populations. In Fig. 2a, $\log C(P)$ is plotted, where C is the smallest confidence level found for a given period P. The dotted line corresponds to the threshold confidence limit.

For the comparison of the two sub-samples, we follow the presentation in Sokal & Rohlf (1981). Since the two samples have generally different variances, the conventional T test should *not* be applied. We use the approximation

$$T_{1,2} = \frac{\bar{f}_1 - \bar{f}_2}{\sqrt{\frac{s_1^2}{n_1} + \frac{s_2^2}{n_2}}} \quad \text{(A1)}$$

A test for the zero hypothesis is assumed, i.e. equal means of the two parent populations of the two samples. $\bar{f}_{1,2}$ are the measured weighted averages of the two samples, and $s_{1,2}$ are the sample standard deviations. The two samples have n_1 and n_2 elements, respectively.

Critical T values with which $T_{1,2}$ in Eq. (A1) is to be compared are obtained from tabulated values T as follows:

$$T_\alpha = \frac{T_{\alpha[\nu_1]}\frac{s_1^2}{n_1} + T_{\alpha[\nu_2]}\frac{s_2^2}{n_2}}{\frac{s_1^2}{n_1} + \frac{s_2^2}{n_2}}, \quad \text{(A2)}$$

where α is the confidence limit, and $T_{\alpha[\nu_i]}$ is the T-value for α and the degree of freedom $\nu_i = n_i - 1$ as read from conventional tables. Notice that Eq. (A2) is a weigthed mean of the two T-values $T_{\alpha[\nu_1]}$ and $T_{\alpha[\nu_2]}$ corresponding to the two degrees of freedom, $n_1 - 1$ and $n_2 - 1$, respectively.

Method B) Point-to-point variability. Rotational modulation ideally shows up as a smooth variation from point to point when the data are plotted in rotation phase. Data folded with an unsuitable period will irregularly fluctuate between different flux levels. A simple and appropriate statistics for the fluxes F_i is therefore defined by

$$\psi^2 = \frac{(F_1 - F_n)^2}{\sigma_{1,n}^2} + \sum_{i=2}^{n} \frac{(F_i - F_{i-1})^2}{\sigma_{i,i-1}^2} \quad \text{(A3)}$$

Here, we chose $\sigma_{i,i-1}^{-2} = (\sigma_i^{-2} + \sigma_{i-1}^{-2})/2$ as a mean of the two involved standard deviations. Eq. (A3) is reminiscent of the χ^2 statistics if the flux of the nearest preceding neighbor, F_{i-1}, were considered to be the expectation value for F_i. This would strictly imply that the test model is a constant function, whereas the purpose of Eq. (A3) is the identification of a function with minimum point-to-point variation. Figure 2b presents the function ψ^2 as a function of folding period P.

The sampling theorem restricts reliable identification of periods to $P > 1.5$ days ($\sim$ twice the shortest relevant sampling interval; in three pairs of observations obtained within $\lesssim 0.75$ days the flux remained constant).

References

Barry D. C., 1988, ApJ 334, 436
Bastian T. S., 1990, Solar Phys. 130, 265
Benz A. O., Güdel M., 1994, A&A 285, 621
Dorren J. D., Guinan E. F., 1994, ApJ 428, 805 = DG94
Dorren J. D., Güdel M., Guinan E. F., 1995, ApJ, in press
Drake S. A., Simon T., Linsky J. L., 1989, ApJS 71, 905
Duquennoy A., Mayor M., 1991, A&A 248, 485
Elias N. M. II, Dorren J. D., 1990a, AJ 100, 818
Elias N. M. II, Dorren J. D., 1990b, IBVS No. 3541
Gliese W., 1969, Catalogue of Nearby Stars. Veröffentl. des Astron. Recheninstituts Heidelberg No. 22
Grenon M., 1993, private communication
Güdel M., 1992, A&A 264, L31, and 1993, A&A 273, 719
Güdel M., 1994, ApJS 90, 743
Güdel M., Benz A. O., 1993, ApJ 405, L63
Güdel M., Schmitt J. H. M. M., 1995, in preparation
Güdel M., Schmitt J. H. M. M., Benz A. O., 1993a, BAAS 25, 874
Güdel M., Schmitt J. H. M. M., Bookbinder J. A., Fleming T. A., 1993b, ApJ 415, 236
Güdel M., Schmitt J. H. M. M., Benz A. O., 1994, Science 265, 933
Güdel M., Schmitt J. H. M. M., Benz A. O., 1995, A&A, in press
Guinan E. F., Dorren J. D., 1992, BAAS 24, 1205
Jeffries R. D., Jewell S. J., 1993, MNRAS 264, 106
Malina R. F., Marshall H. L., Antia B., et al., 1994, AJ 107, 751
Micela G., Sciortino S., Vaiana G. S., et al., 1990, ApJ 348, 557
Pallavicini R., Golub L., Rosner R., et al., 1981, ApJ 248, 279
Pfeffermann E., et al., 1986, SPIE 733, 519
Pounds K. A., Allan D. J., Barber C., et al., 1993, MNRAS 260, 77
Schmitt J. H. M. M., Collura A., Sciortino S., et al., 1990, ApJ 365, 704
Schmitt J. H. M. M., Kahabka P., Stauffer J., Piters A. J. M., 1993, A&A 277, 114
Serio S., Peres G., Vaiana G. S., Golub L., Rosner R., 1981, ApJ 243, 288
Soderblom D. R., 1983, ApJS 53, 1
Soderblom D. R., 1985, AJ 90, 2103
Soderblom D. R., Clements S. D., 1987, AJ 93, 920
Soderblom D. R., Stauffer J. R., MacGregor K. B., Jones B. F., 1993, ApJ 409, 624

Sokal R. R., Rohlf F. J., 1981, Biometry, Freeman and Co., New York, p. 411
Stauffer J. R., Caillault J.-P., Gagné M., Prosser C. F., Hartmann L. W., 1994, ApJS 91, 625
Trümper J., Hasinger G., Aschenbach B., et al., 1993, Nat 349, 579
Turon C., et al., 1992, Hipparcos Input Catalog, ESA SP-1136
van den Oord G. H. J., Mewe R., 1989, A&A 213, 245

This article was processed by the author using Springer-Verlag LaTeX A&A style file *L-AA* version 3.